Influence of the AZO Electrode on ZnO Nanowire Growth by PLI-MOCVD and Related Piezoelectric Performance: Implications for Mechanical Energy Transducers

Quang Chieu Bui, Vincent Consonni, Sarah Boubenia, Guillaume Gay, Corinne Perret, Mohammed Zeghouane, Sebastien Labau, Carmen Jiménez, Hervé Roussel, Xavier Mescot, et al.

Influence of AZO Electrode on ZnO Nanowire Growth by PLI-MOCVD and Related Piezoelectric Performance: Implications for Mechanical Energy Transducers

Quang Chieu Bui,[a,b,c] Vincent Consonni,[b*] Sarah Boubenia,[a] Guillaume Gay,[a] Corinne Perret,[a] Mohammed Zeghouane,[a] Sebastien Labau,[a] Carmen Jiménez,[b] Hervé Roussel,[b] Xavier Mescot,[c] Gustavo Ardila,[c] and Bassem Salem.[a*]

[a] *Université Grenoble Alpes, CNRS, CEA/ LETI Minatec, Grenoble INP, LTM, F-38054 Grenoble, France.*

[b] *Université Grenoble Alpes, CNRS, Grenoble INP, LMGP, F-38000 Grenoble, France.*

[c] *Université Grenoble Alpes, CNRS, Grenoble INP, IMEP-LAHC, F-38000 Grenoble, France.*

ABSTRACT

We investigate the impact of the aluminum-doped zinc oxide (AZO) as an ecofriendly bottom electrode for ZnO nanowire-based mechanical energy transducers. The AZO electrode was grown using the atomic layer deposition (ALD) process, followed by the growth of ZnO nanowires (NWs) using pulsed-liquid injection metal-organic chemical vapor deposition (PLI-MOCVD). The Al dopant concentration is varied to obtain AZO thin films with different morphologies, structural orientations and electrical properties. Depending on the AZO thin film used as the growth platform, the ZnO NW arrays can have a random or vertical alignment. This in turn affected their piezoelectric performance analyzed by piezoresponse force microscopy. Interestingly, the piezoelectric coefficient d_{33} of ZnO NWs grown on the AZO thin films (4.6 – 5.4 pm/V) is higher compared to those grown directly on the heavily doped Si substrate (3 – 3.8 pm/V) with a similar electrical resistivity. The average optical transmittance of a quartz substrate/AZO thin film/ZnO NW structure is of 81.2% in the wavelength range of 400 – 700 nm. The structural and piezoelectric properties of ZnO NWs and their correlation with the AZO thin films used as growth platforms are discussed in detail and open some perspectives to fabricate transparent piezoelectric devices using eco-friendly materials and scaled-up chemical deposition techniques compatible with industrial requirements.

KEYWORDS: ZnO, AZO, Atomic Layer Deposition, Metal-Organic Chemical Vapor Deposition, Nanostructures, Transparent conductive oxide, Piezoelectricity, Nanogenerators.

1. Introduction

ZnO nanowire (NW) structure has many interesting properties such as wide direct bandgap (3.37 eV), high exciton binding energy (60 meV), high flexibility, high light transparency, and high electron mobility, which are suitable for a wide range of applications.[1,2] It has received increasing attention in recent years as a potential candidate for lead-free piezoelectric devices as an abundant, inexpensive, and biocompatible material possessing piezoelectric properties.[3–5] Thanks to its visible light transparency, ZnO NW structure can be combined with other transparent electrodes to develop devices that require both piezoelectric and optical properties, such as touch screen sensors,[6,7] or photocatalytic, photovoltaic as well as innovative piezoelectric applications using the piezo-phototronic effect for performance enhancement.[8–12]

Indium tin oxide (ITO) is usually selected for the transparent electrode thanks to its high electrical conductivity (~10^{-4} Ω.cm) and visible light transmittance (> 85%).[13,14] However, the scarcity and toxicity of indium-based compounds give rise to some concerns related to its supply risk and its cost.[14–16] Other materials that can be used for transparent electrodes are for instance silver NWs,[17] graphene,[18] fluorine-doped zinc oxide (FZO),[19] fluorine-doped tin oxide (FTO),[20] or aluminum-doped zinc oxide (AZO).[21] Among them, AZO is a highly suitable alternative to ITO, as it is composed of abundant elements and considered as a non-toxic material with high electrical conductivity and optical transmittance comparable to ITO.[14,22,23] Using ZnO NWs in combination with AZO electrodes would allow for the fabrication of a transparent piezoelectric device using only non-critical materials. This approach avoids using the materials that may be scarce, toxic, or have significant supply risks, thus ensuring the sustainability of the device.

When the AZO thin film is used as a bottom electrode as well as a growth platform, the deposition proceeds through a homogenous epitaxial growth, in which the surface and structure of the AZO layer can significantly affect the ZnO NW growth process. For instance, S. Pung et al. demonstrated that the growth direction of ZnO NWs is changed depending on the orientation of ZnO thin film used as a platform.[24] Thus, it is necessary to control not only the electrical conductivity and optical transmittance of AZO thin film, but also its structural properties in order to boost the piezoelectric performance. While many researches have showed that the AZO thin film exhibits relevant properties as a transparent electrode that can be used in many applications, there are only very few reports using it in piezoelectric applications, especially through its combination with ZnO NWs.[25]

In this work, we study the possibility to use AZO thin films as an ecofriendly bottom electrode for ZnO NW-based mechanical energy transducers. These transducers can be used in energy harvesting and sensing applications.[26–28] The AZO thin films are initially deposited on Si substrates by atomic layer deposition (ALD) process. The structural and electrical properties of AZO thin films are modified by varying the Al dopant concentration during its growth process. Then, these AZO

electrodes are used as platforms for the subsequent growth of ZnO NWs using PLI-MOCVD process. A schematic of the entire structure is described in **Figure 1**. A comparison of the ZnO NW growth on the AZO thin films to its growth directly on Si substrate is also performed. The morphology, structural properties and piezoelectric performance of ZnO NWs on the AZO thin film are analyzed by field-emission scanning electron microscopy (FESEM), X-ray diffraction (XRD), Raman spectroscopy, and datacube piezoresponse force microscopy (PFM) measurements. In addition, an AZO thin film/ZnO NW structure is grown on a quartz substrate, and its optical transmittance is measured by UV–Vis-NIR spectrophotometry. The impacts of the AZO structural and electrical properties on the ZnO NW growth and piezoelectric performance are discussed in detail.

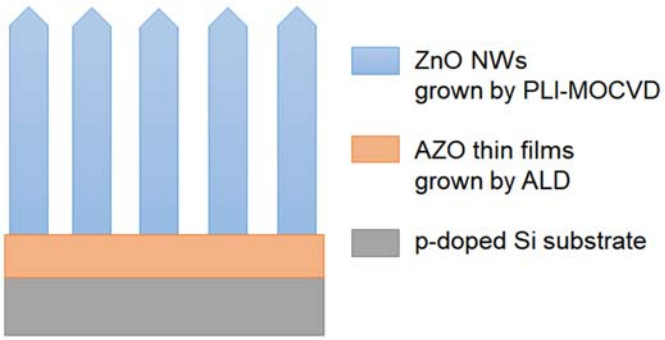

Figure 1: A schematic of Si substrate/AZO thin film/ZnO NW structure and their synthesis processes.

2. Experiment

2.1 AZO electrodes grown by ALD

Initially, AZO thin films were prepared by ALD method using the Cambridge NanoTech Fiji F200 system. Diethylzinc (DEZn) and trimethyl aluminum (TMA) were used as the Zn and Al precursors, respectively. The DEZn/TMA cycle number ratio was modified at 30, 20, and 10 to obtain the AZO thin films with different Al doping concentration, which are labeled as AZO30, AZO20, and AZO10. The water vapor (DI) was used as O precursor. The total cycle number was adjusted for every growth to have the same thickness at around 180 nm. The growths were performed simultaneously on the standard Si (100) with resistivity around 10 Ω.cm, heavily doped p-type Si (100) with the resistivity at 2 x 10^{-3} Ω.cm, and quartz. The thin films on the standard Si substrates were used for the electrical measurements, while the thin films on the heavily doped p-type Si substrates were used for the PFM measurements. The thin films deposited on quartz were used for the optical transmittance measurements. The substrate temperature was maintained at 250 °C.

2.2 ZnO NWs grown by PLI-MOCVD

After the thin film deposition, the as-grown AZO thin films on heavily doped Si substrates were used as platforms for the ZnO NW growths. In addition, the ZnO NW array grown directly on a heavily doped Si substrate was also prepared as reference sample. The ZnO NWs were grown using

PLI-MOCVD technique in an Annealsys MC-200 MOCVD system. The Si substrate, AZO30, AZO 20 and AZO10 thin films were put together in the PLI-MOCVD chamber, and the ZnO NW growths on those platforms were performed simultaneously. The Zn precursor was a solution of DEZn (Sigma-Aldrich) diluted in cyclohexane at 0.4 mol/l. This solution was injected to the reactor chamber at a flow rate of 0.5 g/min with 500 sccm Ar as gas carrier. The O_2 gas as an O precursor was introduced into the chamber with the flow rate set at 300 sccm. The temperature of the substrate and the chamber pressure were kept constant at 700 °C and 3 mbar during the growth, respectively. The growth duration was set at 10 minutes. On each AZO thin film, a small AZO area was covered by a piece of Si in order to protect that area from the ZnO NW deposition. Those AZO areas without ZnO NW deposition were used for electrical connection in the later PFM measurements.

2.3 Characterizations

Structural, chemical, optical and electrical measurements

The morphologies and topographies of AZO thin films and ZnO NWs were studied using a Gemini300 FEI ZEISS-SEM system and a Bruker Dimension Icon atomic force microscope (AFM), respectively. The Al dopant concentrations of AZO thin films were analyzed by parallel angular X-ray photoelectron spectroscopy (XPS). The XPS system includes a customized Thermo Fisher Scientific Theta 300 system equipped with an X-ray source using a monochromatic aluminum anode (1486.6 eV) in ultrahigh vacuum conditions (< 1×10^{-8} Pa). The XRD patterns of samples were investigated by a Bruker D8 Advance diffractometer using Cu $K\alpha_1$ radiation with the Bragg−Brentano configuration. The scanning range was from 20 to 140° on the 2θ-scale. To evaluate the structural orientation of the AZO thin films and ZnO NWs, the texture coefficients C_{hkl}, representing the degree of preferred orientation of a given (hkl) plane within the crystalline structure, were calculated by the following equation:[29]

$$C_{hkl}(\%) = \frac{\frac{I_{hkl}}{I_{0,hkl}} \times 100}{\sum_{i=1}^{N} \frac{I_{h_i k_i l_i}}{I_{0,h_i k_i l_i}}} \quad (1)$$

where I_{hkl} is the hkl peak intensity extracted from the XRD pattern, $I_{0,hkl}$ is the reference hkl peak intensity from the 00-036-1451 file of the International Center for Diffraction Data (ICDD), and N is the number of peaks considered. In addition, the residual homogeneous strain inside the AZO thin films and ZnO NWs at the end of the fabrication process was estimated as follows:

$$\varepsilon_{hs}(\%) = \frac{c - c_o}{c_o} \times 100 \quad (2)$$

where c_o = 5.2066 Å is the theoretical *c*-lattice parameter of wurtzite ZnO according to the 00-036-1451 ICDD file. The actual *c*-lattice parameter value was deduced from the 002 diffraction peak position by using Bragg's law equation:

$$\lambda = 2d \sin\theta \qquad (3)$$

where λ is the wavelength of the Kα1(Cu) source equal to 0.15406 nm, θ is the Bragg angle of the 002 diffraction peak, *d* is the spacing between the (002) planes and equal to half the *c*-lattice parameter in the wurtzite structure of ZnO.

Raman scattering spectra were recorded at room temperature using a Jobin Yvon/Horiba Labram spectrometer and the 488 nm excitation line of an Ar^+ laser. The cross-polarization was used in those Raman scattering measurements to reduce the signals of the silicon substrate. The optical transmittance of the ZnO NW array and AZO thin films deposited on quartz were analyzed using a Perkin Elmer Lambda 950 spectrometer. The AZO thin film resistivity was measured by Van der Pauw measurement method using a home-made station.

Piezoelectric measurements

The piezoelectric properties of ZnO NWs grown on AZO thin films and Si substrate were analyzed by PFM measurements using a Bruker Dimension Icon AFM equipped with a conductive tip (PtSi-NCH, Nanosensors). This tip has high spring constant (~43 N/m), which was employed to reduce the interference of the electrostatic effect during the PFM measurement.[30] Instead of using the contact PFM mode, our measurements were performed in the DataCube PFM mode. In this mode, the tip sequentially approached, touched the sample and withdrew when moving from one position to another. This is to avoid dragging the tip during the scanning, which can bend the NW resulting in contact failure between the tip and the sample. For each position, the contact duration was set at 80 milliseconds. During this time, a 5 V amplitude and 15 kHz frequency AC voltage was applied between the top and the bottom of the sample through the tip and the chuck of the AFM system. Due to the piezoelectric property, the ZnO NW was deformed with respect to the AC voltage. This deformation was recorded, giving the piezoelectric amplitude and phase signals corresponding to the piezoelectric coefficient and the polarity of the ZnO NW, respectively.[30]

3. Results

3.1 Structural properties and resistivity of AZO thin films

Since the AZO30, AZO20 and AZO10 thin films were used as substrates during the ZnO NW growth, they were also affected by the growth conditions in the PLI-MOCVD process. In the reactor chamber, AZO thin films were heated from room temperature to 700 °C at the beginning of the process and were cooled down at the end of the process in Ar atmosphere. When the DEZn and O_2 gas

were introduced to the chamber for the ZnO NW growth, these AZO layers were also exposed to the O_2 gas while being heated at 700 °C for 10 minutes. The pressure inside the reactor chamber was maintained at 3 mbar. This means the AZO layers were annealed throughout the NW growth process, which can affect their properties. To test the structural and electrical properties of AZO thin films after the growth, we repeated the growth process on the as-grown AZO layers using the similar conditions, but without injecting the DEZn precursor. These samples are denoted as annealed AZO thin films. The properties of those annealed AZO layers were measured and compared with the as-grown AZO thin films. **Figure 2** shows the FESEM images of as-grown and annealed AZO thin films.

The top-view images present different morphologies of AZO thin films when the Al dopant concentration is changed, while the cross-sectional-view images show that all thin films have a similar thickness of around 180 nm since the number of cycle was adjusted for every ALD growth. Thus, the effect of AZO thickness on its properties is decoupled from the effect of Al dopant concentration. The incorporation of Al dopants inside the lattice of AZO thin films was confirmed and measured by parallel angular XPS (see **Figure S1**). The Al atomic concentrations of AZO30, AZO20 and AZO10 thin films are found to be 1.1, 2.9 and 6.7%, respectively. **Figure 2** also shows that there is no significant change in the morphology of annealed AZO thin films after the PLI-MOCVD process as compared to the as-grown AZO thin films.

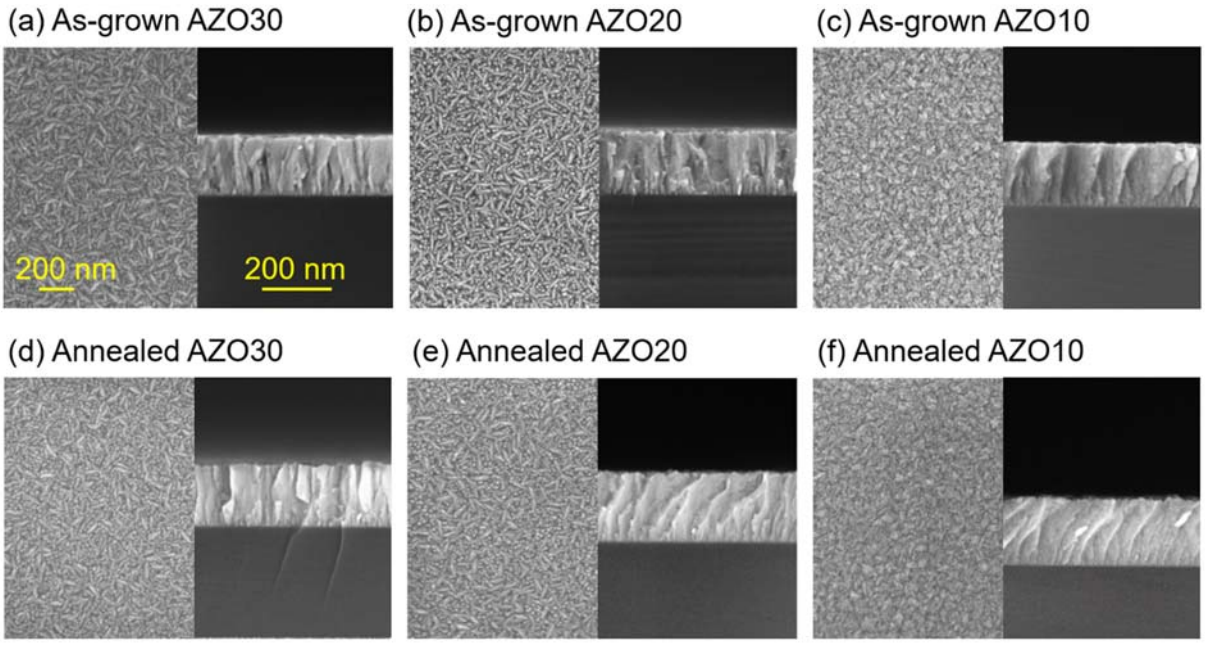

Figure 2: Top-view (left) and cross-sectional-view (right) FESEM images of (a) as-grown AZO30, (b) as-grown AZO20, (c) as-grown AZO10, (d) annealed AZO30, (e) annealed AZO20, and (f) annealed AZO10 thin films.

The XRD patterns of as-grown and annealed AZO thin films are revealed in **Figure 3**. The 100, 002, 101, 110, 102, 103, and 004 diffraction peaks of the ZnO wurtzite structure are observed at

31.8, 34.4, 36.3, 47.5, 56.6, 62.9, and 72.6°, according to the International Center for Diffraction Data (ICDD) file labelled 00-036-145. No peaks of Al-related compound are detected on these XRD patterns, indicating that Al atoms only participate as dopants inside AZO thin films. On the XRD patterns of AZO30 and AZO 20 thin films, it can be seen that the 002 diffraction peak is the most intense one as compared to other ZnO diffraction peaks, revealing that their structures are preferably oriented along the polar *c*-axis. On the other hand, the XRD pattern of AZO10 thin film shows less intense and broader diffraction peaks, expressing a partially crystallized structure. This is due to the fact that a large amount of Al atoms is incorporated into the AZO10 thin film, which causes a large distortion of ZnO lattice and leads to the degradation of its crystal structure.[31,32] To evaluate the degree of preferred orientation along the polar *c*-axis of the different AZO thin films, the 002 texture coefficient were calculated and reached 26.5, 68.2 and 87.8% for AZO10, AZO30 and AZO20 thin films, respectively.

Comparing to the XRD patterns of as-grown AZO thin films in **Figure 3a**, the XRD patterns of annealed AZO thin films in **Figure 3b** are similar. This comparison along with the FESEM images in **Figure 2** shows that the annealing during the PLI-MOCVD process has insignificant effect on the structural properties of AZO thin films. The residual homogeneous strain of as-grown and annealed AZO thin films was also evaluated based on the position of the 002 diffraction peaks in the XRD patterns.[30] The residual homogeneous strain is found to slightly increase from -0.56, -0.83 and -1.77% to -0.67, -0.99 and -2.05% in AZO30, AZO20 and AZO10 thin films, respectively, following the annealing during the PLI-MOCVD process. This could be due to the adsorption of oxygen during the annealing at high temperature inside the PLI-MOCVD chamber, which have been reported to create defects or to induce a local segregation of Al atoms.[33,34]

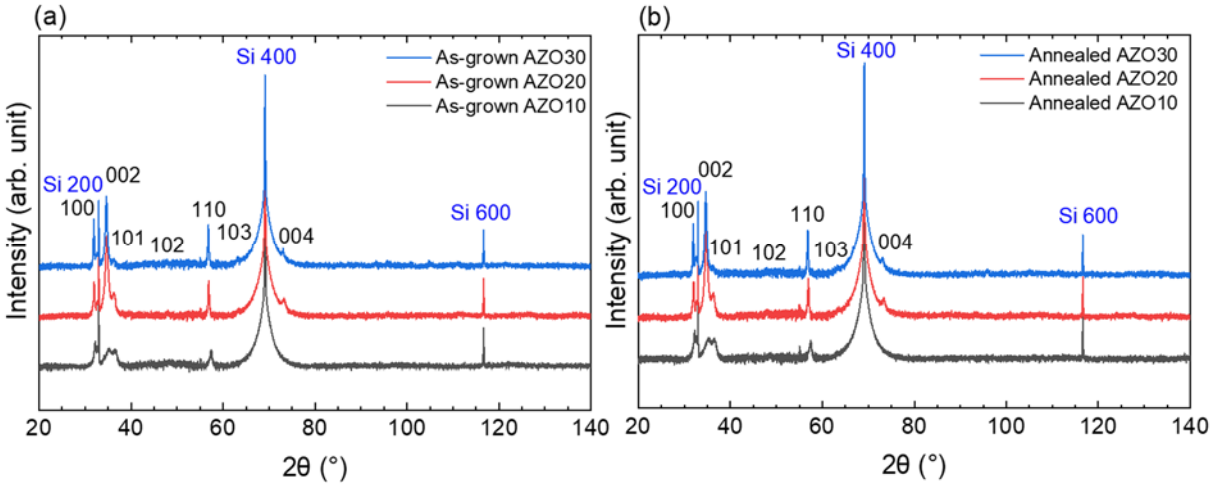

Figure 3: XRD patterns of (a) as-grown and (b) annealed AZO thin films. The intensity was plotted in logarithmic scale.

Different from the structural properties, the electrical measurements show that the electrical resistivity of AZO30 and AZO20 thin films is increased by 1 order of magnitude (from 0.6 – 0.7 x 10^{-3} to around 5 x 10^{-3} Ω.cm) after the annealing. Since the AZO thin films are annealed under O_2 atmosphere, this could be due to i) the adsorption of oxygen at grain boundaries trapping free electrons,[34] or to ii) the local segregation of Al atoms reducing the concentration of shallow donors formed by Al_{Zn} defects as well as the charge carrier density.[33] On the other hand, the electrical resistivity of AZO10 thin film is found to be around 5.5 x 10^{-3} Ω.cm and it remains the same after annealing. This could be due to the fact that the charge carriers inside the AZO10 thin film had been trapped even before annealing due to its partially crystallized structure. Nevertheless, the electrical resistivity of AZO thin films after annealing is still decent and comparable to the electrical resistivity of the heavily doped Si substrate, which is around 2 x 10^{-3} Ω.cm.

3.2 Morphology of ZnO NWs grown on AZO thin films

The FESEM images in **Figure 4** show that the ZnO NWs formed on Si substrate, AZO30 and AZO20 thin films are well-aligned vertically, but not on the AZO10 thin film. In our previous result,[30] the ZnO NW formation on Si substrate was found to be a non-epitaxial growth. In that growth, a very thin polycrystalline ZnO layer was formed at the onset of the nucleation process, followed by the prevalence of the growth along the polar *c*-axis over the other growth directions at high growth temperature, leading to the vertical ZnO NW growth. In contrast, the ZnO NW formation on the AZO layer proceeds through a homogeneous epitaxial growth, where the direction of the initial layer strongly affects the direction of the structure grown on top of it.

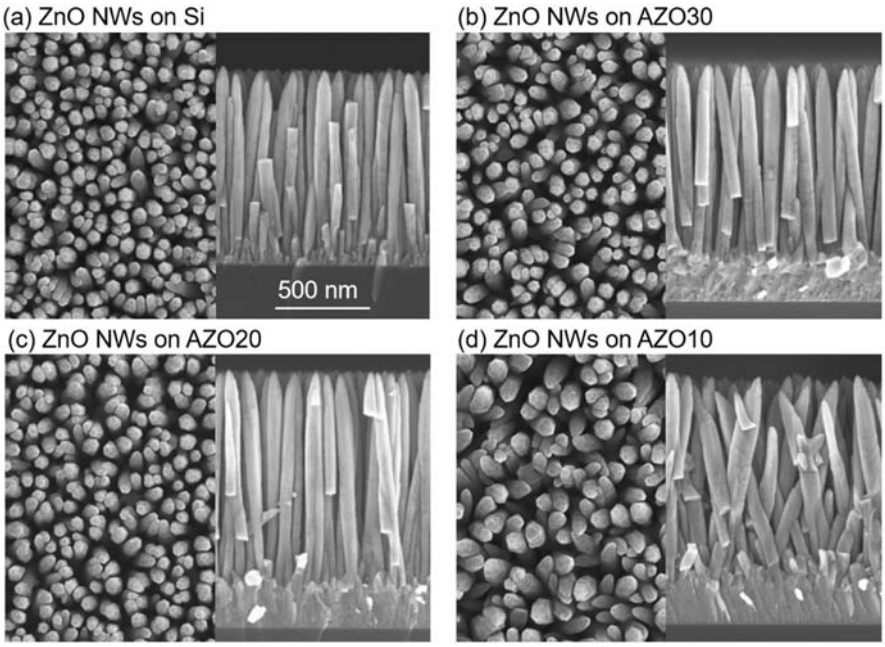

Figure 4: Top-view (left) and cross-sectional-view (right) FESEM images of ZnO NWs grown by PLI-MOCVD on (a) Si substrate, (b) AZO30, (c) AZO20 and (d) AZO10 thin films.

Since the AZO30 and AZO20 thin films exhibit a strong growth texture along the polar *c*-axis as shown by the XRD patterns in **Figure 3**, ZnO NWs grown by PLI-MOCVD on these thin films are also vertically developed. In contrast, the weak growth texture of the AZO10 thin film influences the growth direction of ZnO NWs grown by PLI-MOCVD that leads to its random inclination. A similar observation was reported in ref.[24], where ZnO NWs were grown on AZO templates by chemical vapor deposition process. The length and diameter of ZnO NWs were measured from the cross-sectional FESEM images and are presented in **Table 1**.

Table 1: Lengths and diameters of ZnO NWs grown by PLI-MOCVD on Si substrate and AZO thin films.

Sample	Length (nm)	Diameter (nm)
ZnO NWs on Si	1029 ± 83	72 ± 10
ZnO NWs on AZO30	1072 ± 92	77 ± 14
ZnO NWs on AZO20	1174 ± 74	77 ± 13
ZnO NWs on AZO10	1092 ± 63	95 ± 16

The length of ZnO NWs grown on the different AZO thin films and on Si substrate is above 1 µm and similar, but their diameter when grown on the AZO10 thin film is notably larger. As the ZnO NWs on the AZO10 thin film were grown with different inclination angles, these NWs can cross and merge into bigger NWs. These results demonstrate that the surface of AZO thin films have a strong impact on the nucleation process of ZnO, which in turn affects the formation process of NWs in the subsequent growth step. Interestingly, we also performed a comparison between the ZnO NW growth by PLI-MOCVD process on the Zn-polar ZnO single crystal (from Crystec) and on the AZO20 thin film (see **Figure S2**). The result shows that the ZnO NW arrays grown on the AZO20 thin film oriented along the polar *c*-axis achieves a vertical alignment that is similar to the ZnO NW arrays grown on the ZnO single crystal, which is a more expensive substrate offering less integration perspectives for piezoelectric devices.

3.3 Structural and optical properties of ZnO NWs/AZO thin film structure

Figure 5a shows the XRD patterns of ZnO NWs grown on the Si substrate and AZO thin films. Besides the diffraction peaks of Si substrate, other diffraction peaks are attributed to the ZnO wurtzite structure, according to the ICDD file labelled 00-036-1451. In all samples, the 002 diffraction peak exhibits a significantly higher intensity compared to other diffraction peaks, indicating that ZnO NWs are grown along the polar *c*-axis during the PLI-MOCVD process. It is also worth noticing in **Figure 5b** that most of the diffractions peaks exhibit two components: the one at higher θ value is the diffraction peak assigned to the AZO thin film grown by ALD, and the other one at lower θ value is the diffraction peak attributed to the ZnO structure formed by MOCVD. In **Figure 5a**, the XRD pattern of ZnO NWs grown on the AZO10 thin film shows many different diffraction peaks. The 104,

105 and 106 diffraction peaks located at 81.4, 104.1 and 136.5 ° were not seen in the XRD pattern of the AZO10 film due to its low thickness, but here they are also detected. The increase in the intensity of these diffraction peaks after the PLI-MOCVD process reveals that different orientation growths continued to develop on the surface of the AZO10 thin film. This again indicates the poor orientation of the AZO10 thin film that leads to the formation of randomly inclined ZnO NWs. Consequently, the intensity of the 002 diffraction peaks of ZnO NWs is lower when grown on the AZO10 thin film than on the other AZO thin films. This is due to the fact that the XRD patterns were recorded in Bragg–Brentano configuration, in which only the planes that are parallel to the substrate get their signals collected.[35] Thus, only the (002) planes of vertically aligned ZnO NWs are shown in the XRD pattern, while the (002) planes of other inclined ZnO NWs are not recorded.

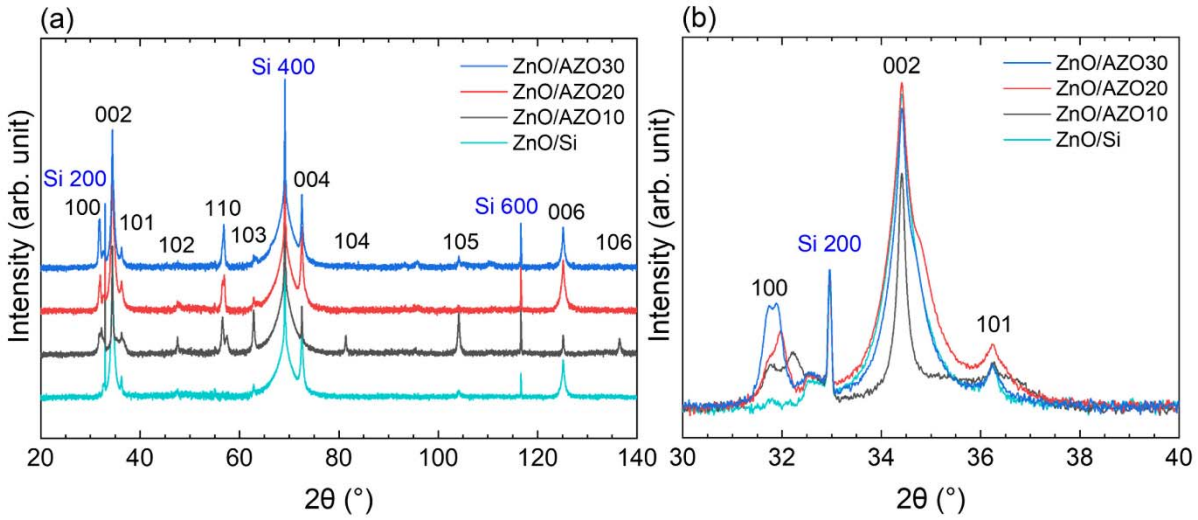

Figure 5: (a) XRD patterns of ZnO NWs grown by PLI-MOCVD on Si substrate and AZO thin films; (b) Zoom-in in the area of interest ranging from 30 to 40° in the XRD patterns. The intensity was plotted in logarithmic scale.

The 002 texture coefficients and residual homogeneous strains of ZnO NWs were also extracted from the XRD patterns (see **Figure S3**). The 002 texture coefficients of ZnO NWs on the Si substrate, AZO30 and AZO20 thin films are higher than 99 %. This value on the AZO10 thin film is also higher than 97%. This confirms that the ZnO NWs were grown by PLI-MOCVD along the polar *c*-axis. The residual homogeneous strains of ZnO NWs are close to 0 despite the fact that their lattice parameters are expected to slightly differ from the one of AZO thin films, indicating the efficient strain relaxation process originating from the NW geometry.

The comparison of the Raman spectra of the as-grown and annealed AZO thin films and of ZnO NWs was also carried out (see **Figure S4**). The Raman spectra of AZO thin films before and after annealing are similar, which again shows no evidence of change in their structure. In contrast, the remarkably high intensities of the E_2^{low} and E_2^{high} lines on the Raman spectra of ZnO NWs emphasize their superior crystallinity as compared to AZO thin films. Those Raman spectra also show that the

strong signals of C-C bonds caused by carbon impurities[30] only appear on ZnO NWs grown by PLI-MOCVD process, but not in AZO thin films grown by ALD despite the fact that the DEZn chemical precursor was used as a source of Zn in both techniques. This indicates that those carbon impurities are mostly removed after the ALD process and hence they do not contribute to the high electrical conductivity of AZO thin films.

The ZnO NW growth by PLI-MOCVD was also performed on the AZO20 thin film, which was deposited on quartz substrate by ALD. The optical transmittance is presented in **Figure 6**. It is seen that the optical transmittance decreases after the ZnO NWs were grown on the AZO20 thin film, as compared to the as-grown AZO20 thin film. However, the ZnO NWs/AZO20 thin film structure still has a high average optical transmittance in the range of 400 – 700 nm, which is around 81.2%. For comparison, ZnO nanorods grown on ITO-coated polyethersulfone (PES) substrate were reported in ref.[6], showing an optical transmittance varying from 60 to 80% in the range of 400 – 700 nm. A transparent piezoelectric touch sensor based on ZnO NWs/BaTiO layer with carbon nanotubes–silver NWs as an electrode was developed in ref.[7], for which the optical transmittance is of 81% at 550 nm-wavelength. This shows that the present ZnO NWs/AZO20 thin film structure is highly suitable for visible-blind and transparent optical applications.

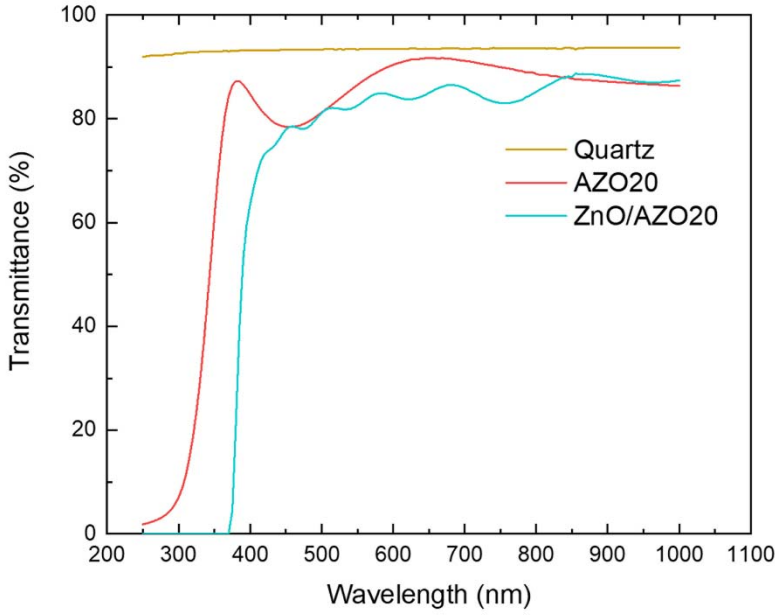

Figure 6: Optical transmittance of AZO20 thin film and ZnO NWs/AZO20 thin film grown on quartz substrate. The AZO20 thin film was first grown on quartz by ALD, and the ZnO NWs were then grown on the AZO20 thin film by PLI-MOCVD.

3.4 Piezoelectric responses of ZnO NWs on AZO thin films

The PFM measurements were performed on ZnO NWs grown on the AZO thin films and Si substrates using 2 setups. In the 1st setup, the samples were in contact with the chuck of the AFM-PFM system (**Figure 7a**). The voltage was applied directly on the heavily doped Si substrate, through the AZO layer at the bottom and the conductive tip at the top. In this setup, the heavily doped Si substrates

were used as the bottom electrodes. To verify that our AZO thin films are able to be used as bottom electrodes for the piezoelectric applications, a 2nd setup was used for the PFM measurement. In this 2nd setup, the heavily doped Si substrate was electrically isolated with the chuck by an empty plastic box placed between them (**Figure 7b**). The voltage was applied on the AZO layer through a copper (Cu) tape. Thus, the voltage was applied directly to the AZO layer instead of indirectly through the Si substrate. Then, datacube PFM measurement was performed.

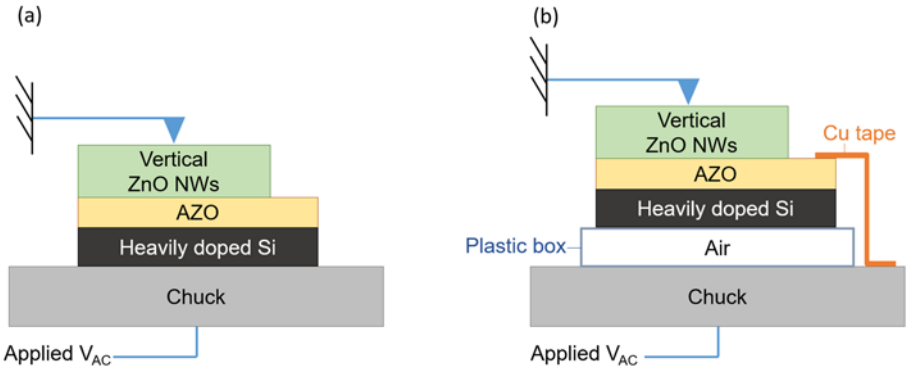

Figure 7: Schematic of the setups for PFM measurements. (a) In the 1st setup, the voltage was applied to the ZnO NW array through the heavily doped Si substrate and AZO layer. (b) In the 2nd setup, the voltage was applied to the ZnO NW array through a Cu tape and the AZO layer.

Figure 8 shows the topography, piezoelectric amplitude and phase images of ZnO grown on Si substrate and AZO thin films recorded by datacube PFM measurement with the 1st setup. In these images, the piezoelectric amplitude is proportional to the piezoelectric coefficient, while the phase indicates the polarity of the ZnO structures.[30] Similar to our results shown in ref.[30], the phase responses of ZnO NWs grown by PLI-MOCVD are positive indicating the Zn-polarity (**Figures 8i-l**). The negative phase response comes from the artifacts generated when the AFM tip scans on the void between NWs. A data treatment was carried out to remove these artifact signals. In this data treatment, the data points with phase value > 50° were kept, while other data points were removed.

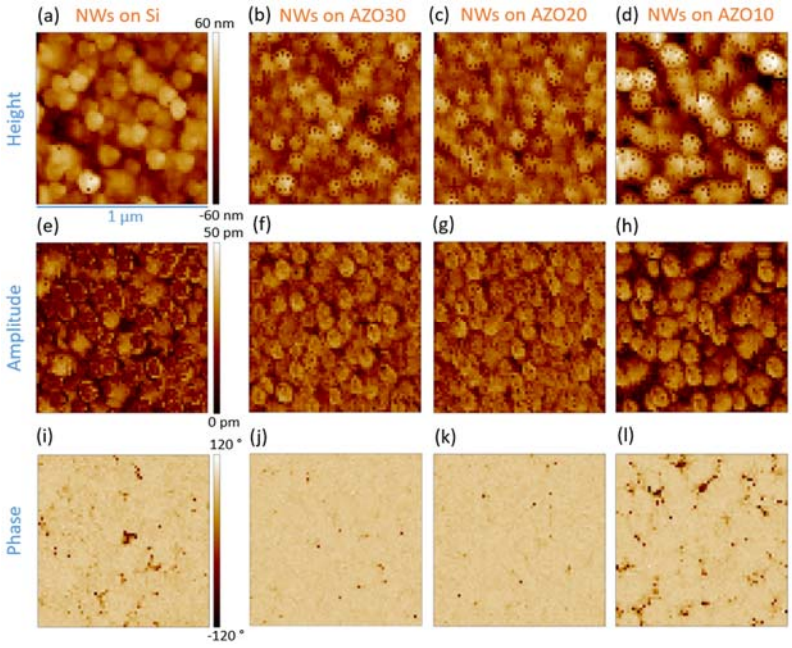

Figure 8: Topography of ZnO NWs on (a) heavily doped Si substrate, (b) AZO30, (c) AZO20, and (d) AZO10 thin films. Piezoelectric amplitude of ZnO NWs on (e) heavily doped Si substrate, (f) AZO30, (g) AZO20, and (h) AZO10 thin films. Piezoelectric phase of ZnO NWs on (i) heavily doped Si substrate, (j) AZO30, (k) AZO20, and (l) AZO10 thin films. The PFM measurements were performed in the 1st setup.

Figures 9a-d shows the amplitude histograms after data treatment of ZnO NWs grown on the Si substrate and AZO thin films measured in the 1st setup, where the voltage was applied through the Si substrate and the AZO layer. The results reveal that while the amplitude is varied from 0 to 37 pm on all NW samples, their amplitude distributions are different. In the histogram of NWs grown on Si substrate (**Figure 9a**), the piezoelectric amplitude with the highest count, namely most frequent value of the distribution (the mode), is around 15 – 19 pm. Interestingly, this mode value of NWs grown on all three AZO layers is higher than on Si substrates, which is around 23 – 27 pm (**Figures 9b-d**). The higher amplitude of NWs grown on AZO thin films compared to NWs grown directly on Si substrate is also illustrated by brighter domains shown in their piezoelectric amplitude images (**Figures 8e-h**). Since the amplitude of applied voltage is 5 V, the piezoelectric coefficient d_{33} can be estimated as lying in the ranges of 3 – 3.8 pm/V for ZnO NWs grown directly on Si substrate, and of 4.6 – 5.4 pm/V for ZnO NWs grown on AZO thin films. These piezoelectric coefficient d_{33} measured in the present ZnO NWs are still moderate as compared to other reports, where they lie in the range from 9.9 to 44.3 pm/V as shown in refs.[36–38] This could be due to the presence of impurities that were incorporated into ZnO NWs during the PLI-MOCVD growth, which screened the piezoelectric response.

Among AZO layers, the piezoelectric amplitude histogram on AZO10 thin film has a broad distribution, which stretches to the low piezoelectric amplitude value (**Figure 9d**). Correspondingly,

the mode value in the histogram of NWs on AZO10 thin film consists of 30.9 % of its distribution, while it is 48.2 % on AZO20 and AZO30 thin films. This can be explained by the randomly inclined NWs on AZO10 thin film. When the AFM tip approached the NW on AZO20 and AZO30 thin films during the datacube PFM measurement, it was in contact with the NW tip and the applied electric field direction coincided with the polar *c*-axis of the NWs thanks to their well-aligned NW array. In contrast, since there are many inclined NWs on AZO layer, the AFM tip can touch the NWs at their sidewall. At that position, the piezoelectric measurement was carried out on the ZnO semi-polar plane instead of the polar plane, resulting in the lower piezoelectric amplitude.

Similarly, the datacube PFM measurements were performed on ZnO NWs grown on the AZO thin films with the 2nd setup, where the bottom electrical contact only went through the Cu tape and AZO layer while the Si substrates were isolated. The data treatment was also applied to remove the artifact signals at the void between NWs. Their piezoelectric amplitude histograms were shown in **Figures 9e-g**. The results show that the amplitude histograms of ZnO NWs grown on the AZO30 and AZO20 thin films in the 2nd setup (**Figures 9e-f**) are similar to their histograms in the 1st setup (**Figures 9b-c**). The amplitude histogram of ZnO NWs on the AZO10 thin film measured in the 2nd setup (**Figure 9g**) also has a broad distribution compared to the 1st setup (**Figure 9d**) due to the inclined NWs, but it is shifted to a lower value.

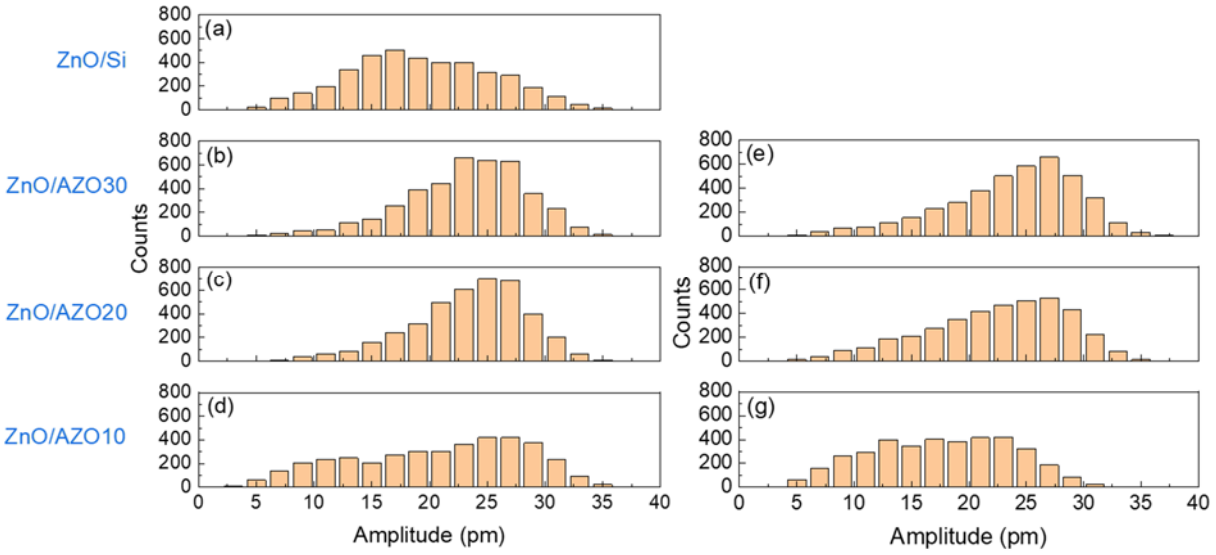

Figure 9: Piezoelectric amplitude histogram after data treatment with the 1st setup of ZnO NWs grown on (a) heavily doped Si substrate, (b) AZO30, (c) AZO20 and (d) AZO10 thin films. Piezoelectric amplitude histogram after data treatment with the 2nd setup of ZnO NWs grown on (e) AZO30, (f) AZO20 and (g) AZO10 thin films.

4. Discussion

To have an overview, the average piezoelectric amplitude of all ZnO NWs measured using the 1st and 2nd experimental setups was calculated and shown in **Figure 10**. In the 1st setup, the average piezoelectric amplitude value is of 19.4 pm for ZnO NWs grown directly on Si substrate, while it is of 23.2, 23.4 and 20.7 pm for ZnO NWs grown on the AZO30, AZO20 and AZO10 thin films, respectively. In the 2nd setup, this value is of 23.7, 22.4 and 17.6 pm for ZnO NWs grown on the AZO30, AZO20 and AZO10 thin films, respectively. It can be seen that the piezoelectric amplitude is higher on ZnO NWs grown on the AZO thin films compared to those grown directly on Si substrate.

Since all the NWs were grown simultaneously on the Si substrate and AZO thin films in the MOCVD chamber, the difference in the piezoelectric amplitude among samples was not caused by the growth atmosphere. Besides, the XRD patterns in **Figure 5** show that the ZnO NWs on Si substrate have a very high polar *c*-axis orientation similar to the ZnO NWs on other AZO thin films. In detail, the ZnO NWs on Si substrate exhibit the highest 002 texture coefficient (99.9%), followed by the ZnO NWs on AZO20 (99.7%), AZO30 (99.2%) and AZO10 thin films (97%), as shown in **Figure S3**. Although a higher *c*-axis orientation typically leads to a larger piezoelectric amplitude, the higher piezoelectric amplitude of ZnO NWs grown on AZO thin films compared those grown directly on Si substrate as shown in **Figures 9** and **10** indicates that the introduction of the AZO layer has a more significant impact on the piezoelectric amplitude of ZnO NWs, while a minor difference in the texture coefficient has little effect.

Regarding the electrodes, because the electrical resistivity of Si and AZO thin films are similar and of around 2 – 5 x 10^{-3} **Ω**.cm, the applied voltage at the bottom electrical contact should be the same for all samples during the PFM measurement. Regarding the effect of heterostructures on the piezoelectric performance, Q. Wang et al. have shown that free electrons can be trapped at ZnO-CuO heterojunction, resulting in enhancing the piezoelectric output.[39] Similarly, K. Pradel et al. demonstrated that the piezoelectric output was significantly increased by two ZnO layers containing different dopants.[40] The p-Si/ZnO/n-AZO heterostructure was also demonstrated by G. Li et al..[41] In our work, a P-N junction formed between the p-doped Si-substrate and the ZnO NWs could lead to a higher piezoelectric amplitude compared to ZnO/AZO junction, but the present experimental results show the opposite trend. The other factor that could also affect the results is the dimensions of NWs. For instance, the NWs grown on AZO thin films exhibit a slightly greater length (**Table 1**), leading to a more effective impact of surface traps depleting the NW from its surface and thus enhancing the piezoelectric performance.[42–44] Conversely, the NWs on the AZO10 thin film are notably larger than others, in this case, the surface traps induced depletion is less effective resulting in a decreased piezoelectric performance.[43]

Moreover, the piezoelectric amplitude of ZnO NWs grown on AZO thin films was also measured in the 2nd setup where the Si substrates were electrically isolated, and compared with their amplitude measured in the 1st setup where the applied voltage went through the Si substrate and AZO thin film (**Figure 7**). The piezoelectric amplitude of ZnO NWs grown on the AZO30 and AZO20 thin films is similar in both setups (**Figures 9b-c**, **e-f** and **Figure 10**), demonstrating that an efficient electrical contact between the copper tape and AZO layer was established. This also indicates that those AZO thin films have a good electrical conductivity to be used as an electrode in piezoelectric applications. In contrast, the piezoelectric amplitude of ZnO NWs on the AZO10 thin film measured in the 2nd setup is lower compared to the 1st setup (**Figures 9d**, **g** and **Figure 10**). While the electrical resistivity of the AZO10 thin film is similar to the electrical resistivity of the AZO20 and AZO30 thin films after the NW growth process (around 5 x 10^{-3} Ω.cm), the reason could be due to the poor electrical contact between the copper tape and partially crystallized AZO10 thin film. This could lead to a drop of the applied voltage at the bottom electrode and hence a lower measured piezoelectric amplitude of NWs on the AZO10 thin film. This result shows that a good electrical contact is important for piezoelectric devices. Furthermore, the more uniform and higher average piezoelectric amplitude values of ZnO NWs on the AZO30 and AZO20 thin films suggest that they can have better piezoelectric performance.

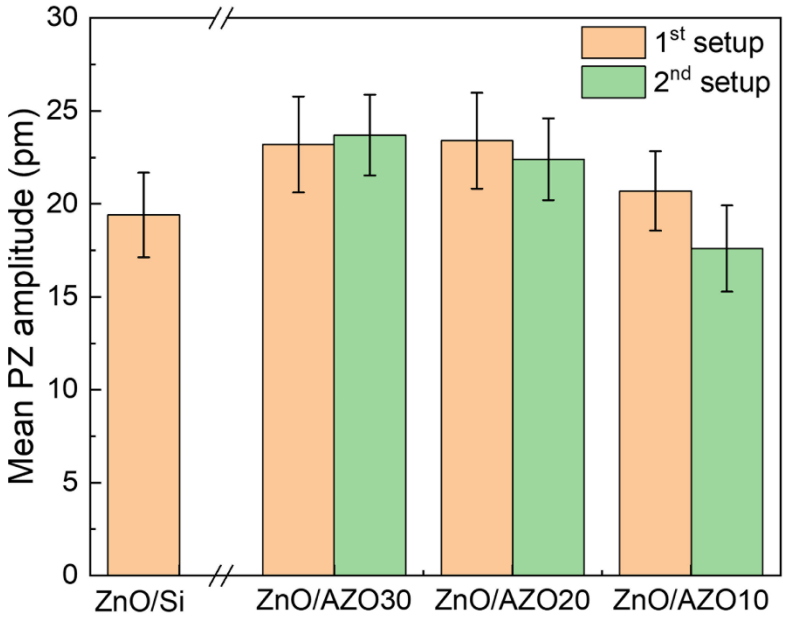

Figure 10: Mean piezoelectric amplitudes after data treatment of ZnO NWs grown by PLI-MOCVD on heavily doped p-type Si substrate, AZO30, AZO20 and AZO10 thin films.

5. Conclusion

In summary, we have demonstrated the AZO thin film deposition by ALD, followed by the ZnO NW growth by PLI-MOCVD process. By modifying Zn/Al precursor cycle ratio in ALD process,

the Al dopant concentrations of AZO thin films have been varied from 1.1 to 6.7%. Simultaneously, the structural orientations of these AZO thin films have also been changed, which have strongly influenced the subsequent growth direction of ZnO NWs. As a consequence, the vertically aligned ZnO NW arrays have been formed on the highly *c*-axis oriented AZO30 and AZO20 thin films, while the randomly inclined ZnO NWs have been grown on the partially crystallized AZO10 thin film. This has in turn affected the piezoelectric amplitude of the ZnO NW arrays. Among the NW arrays grown on AZO thin films, the NW arrays grown on the highly *c*-axis oriented AZO thin films have more uniform and higher piezoelectric amplitude compared to those grown on the partially crystallized AZO thin film. Interestingly, the PFM measurements have also revealed that the piezoelectric amplitude of ZnO NWs grown on the AZO thin film are higher compared to those grown directly on Si substrate. The reason could be due to a depletion layer formation at the AZO layer/ZnO NW interface, which can reduce the free electron movement inside ZnO NWs, leading to the increase the piezoelectric performance. The highest average piezoelectric coefficient d_{33} is achieved on ZnO NWs grown on the highly *c*-axis oriented AZO30 and AZO20 thin films, which is at around 4.5 - 4.7 pm/V. These results show that the ZnO NW piezoelectric performance is significantly affected by the properties of the AZO thin film used as a growth platform, which can finely be optimized during the ALD process. Moreover, the average optical transmittance of 81.2% of the quartz substrate/AZO thin film/ZnO NW structure in the visible light region shows that they are relevant candidates for optoelectronic devices. The combination of these materials and of the ALD and MOCVD techniques that can be extended to industrial scale production show a high potential for developing eco-friendly mechanical energy transducers that are suitable for energy harvesting and sensing applications.

Associated Content

Supporting Information

Average concentration of Al atoms inside the as-grown AZO30, AZO20 and AZO10 thin films measured by XPS (Figures S1); FESEM images of the ZnO NWs grown by PLI-MOCVD on Zn-polar ZnO substrate and AZO20 thin film (Figures S2); 002 texture coefficient and residual homogeneous strain of ZnO NWs grown by PLI-MOCVD on Si substrate and AZO thin films (Figures S3); Raman scattering spectra of as-grown AZO thin films grown by ALD, annealed AZO thin films grown by ALD, and ZnO NWs grown by PLI-MOCVD on Si substrate and AZO layers (Figure S4)

Author Information

Corresponding Authors

Vincent Consonni − *Université Grenoble Alpes, CNRS, Grenoble INP, LMGP, F-38000 Grenoble, France;*

Email: vincent.consonni@grenoble-inp.fr

Bassem Salem – *Université Grenoble Alpes, CNRS, CEA/ LETI Minatec, Grenoble INP, LTM, F-38054 Grenoble, France*;

Email: bassem.salem@cea.fr

Author Contributions

The manuscript was written through contributions of all authors. All authors have given approval to the final version of the manuscript.

Funding Sources

This work was financially supported by the French National Research Agency in the framework of the "Investissements d'avenir" program (ANR-15-IDEX-02) through the project CDP NEED. Q.C.B. held a doctoral fellowship from the project CDP NEED. The authors further acknowledge the financial support from the French National Research Agency through the project SCENIC (ANR-20-CE009-0005) and the CNRS Renatech Network through the "Plateforme Technologique Amont" in a cleanroom environment. This research has also benefited from some of the characterization equipments of the Grenoble INP-CMTC platform and from the facilities and expertise of the OPE)N(RA characterization platform of FMNT (FR 2542, fmnt.fr) supported by CNRS, Grenoble INP and UGA.

Notes

The authors declare no competing financial interest.

Acknowledgements

The authors are further grateful to Isabelle Gelard, Odette Chaix-Pluchery and Laurent Terrier, LMGP, Grenoble, France, for their assistance in FESEM, Raman spectroscopy and UV–Vis-NIR spectrophotometry, respectively.

References

(1) Özgür, Ü.; Alivov, Y. I.; Liu, C.; Teke, A.; Reshchikov, M. A.; Doğan, S.; Avrutin, V.; Cho, S. J.; Morkoç, H. A Comprehensive Review of ZnO Materials and Devices. *J. Appl. Phys.* **2005**, *98* (4), 1–103. https://doi.org/10.1063/1.1992666.

(2) Kołodziejczak-radzimska, A.; Jesionowski, T. Zinc Oxide—From Synthesis to Application: A Review. *Materials (Basel).* **2014**, *7* (4), 2833–2881. https://doi.org/10.3390/ma7042833.

(3) Wang, Z. L. Towards Self-Powered Nanosystems : From Nanogenerators to Nanopiezotronics. *Adv. Funct. Mater.* **2008**, *18*, 3553–3567. https://doi.org/10.1002/adfm.200800541.

(4) Goel, S.; Kumar, B. A Review on Piezo-/ Ferro-Electric Properties of Morphologically Diverse

ZnO Nanostructures. *J. Alloys Compd.* **2020**, *816*, 152491. https://doi.org/10.1016/j.jallcom.2019.152491.

(5) Le, A. T.; Ahmadipour, M.; Pung, S. A Review on ZnO-Based Piezoelectric Nanogenerators : Synthesis, Characterization Techniques, Performance Enhancement and Applications. *J. Alloys Compd.* **2020**, *844* (5), 156172. https://doi.org/10.1016/j.jallcom.2020.156172.

(6) Choi, M. Y.; Choi, D.; Jin, M. J.; Kim, I.; Kim, S. H.; Choi, J. Y.; Lee, S. Y.; Kim, J. M.; Kim, S. W. Mechanically Powered Transparent Flexible Charge-Generating Nanodevices with Piezoelectric ZnO Nanorods. *Adv. Mater.* **2009**, *21* (21), 2185–2189. https://doi.org/10.1002/adma.200803605.

(7) Kang, M. K.; Park, J. H.; Lee, K. Il; Cho, J. W.; Bae, J.; Ju, B. K.; Lee, C. S. Fully Flexible and Transparent Piezoelectric Touch Sensors Based on ZnO Nanowires and BaTiO3-Added SiO2 Capping Layers. *Phys. Status Solidi Appl. Mater. Sci.* **2015**, *212* (9), 2005–2011. https://doi.org/10.1002/pssa.201431829.

(8) Liu, C.; Peng, M.; Yu, A.; Liu, J.; Song, M.; Zhang, Y.; Zhai, J. Interface Engineering on P-CuI/n-ZnO Heterojunction for Enhancing Piezoelectric and Piezo-Phototronic Performance. *Nano Energy* **2016**, *26*, 417–424. https://doi.org/10.1016/j.nanoen.2016.05.041.

(9) Song, M.; Liu, Y.; Yu, A.; Zhang, Y.; Zhai, J.; Wang, Z. L. Flexible Li-Doped ZnO Piezotronic Transistor Array for in-Plane Strain Mapping. *Nano Energy* **2019**, *55*, 341–347. https://doi.org/10.1016/j.nanoen.2018.11.013.

(10) Pan, L.; Sun, S.; Chen, Y.; Wang, P.; Wang, J.; Zhang, X.; Zou, J. J.; Wang, Z. L. Advances in Piezo-Phototronic Effect Enhanced Photocatalysis and Photoelectrocatalysis. *Adv. Energy Mater.* **2020**, *10* (15), 1–25. https://doi.org/10.1002/aenm.202000214.

(11) Zhang, Y.; Yang, L.; Zhang, Y.; Ding, Z.; Wu, M.; Zhou, Y.; Diao, C.; Zheng, H.; Wang, X.; Wang, Z. L. Enhanced Photovoltaic Performances of La-Doped Bismuth Ferrite/Zinc Oxide Heterojunction by Coupling Piezo-Phototronic Effect and Ferroelectricity. *ACS Nano* **2020**, *14* (8), 10723–10732. https://doi.org/10.1021/acsnano.0c05398.

(12) Zheng, Q.; Peng, M.; Liu, Z.; Li, S.; Han, R.; Ouyang, H.; Fan, Y.; Pan, C.; Hu, W.; Zhai, J.; Li, Z.; Wang, Z. L. Dynamic Real-Time Imaging of Living Cell Traction Force by Piezo-Phototronic Light Nano-Antenna Array. *Sci. Adv.* **2021**, *7* (22), 1–9. https://doi.org/10.1126/sciadv.abe7738.

(13) Ellmer, K. Past Achievements and Future Challenges in the Development of Optically Transparent Electrodes. *Nat. Photonics* **2012**, *6*, 809–817. https://doi.org/10.1038/NPHOTON.2012.282.

(14) Kawajiri, K.; Tahara, K.; Uemiya, S. Lifecycle Assessment of Critical Material Substitution: Indium Tin Oxide and Aluminum Zinc Oxide in Transparent Electrodes. *Resour. Environ. Sustain.* **2022**, *7* (April 2021), 100047. https://doi.org/10.1016/j.resenv.2022.100047.

(15) Lim, C. H.; Han, J.; Cho, H.; Kang, M. Studies on the Toxicity and Distribution of Indium Compounds According to Particle Size in Sprague-Dawley Rats. *Toxicalogical Reseach* **2014**, *30* (1), 55–63.

(16) Badding, M. A.; Fix, N. R.; Orandle, M. S.; Barger, M. W.; Dunnick, K. M.; Cummings, K. J.; Leonard, S. S. Pulmonary Toxicity of Indium-Tin Oxide Production Facility Particles in Rats. *J. Appl. Toxicol.* **2015**, *36* (4), 618–626. https://doi.org/10.1002/jat.3253.

(17) Madeira, A.; Papanastasiou, D. T.; Toupance, T.; Servant, L.; Bellet, D.; Goldthorpe, I. A. Rapid Synthesis of Ultra-Long Silver Nanowires for High Performance Transparent Electrodes. *Nanoscale Adv.* **2020**, *2* (9), 3804. https://doi.org/10.1039/d0na00392a.

(18) Rana, K.; Singh, J.; Ahn, J. A Graphene-Based Transparent Electrode for Use in Fl Exible

Optoelectronic Devices. *J. Mater. Chem. C* **2014**, *2* (15), 2646. https://doi.org/10.1039/c3tc32264e.

(19) Tuan, A.; Pham, T.; Minh, N.; Kieu, O.; Le, T.; Hoang, D. Van; Huu, T.; Bach, T.; Cao, V. Journal of Science : Advanced Materials and Devices High-Mobility Sputtered F-Doped ZnO Films as Good-Performance Transparent-Electrode Layers. *J. Sci. Adv. Mater. Devices* **2021**, *6* (3), 446–452. https://doi.org/10.1016/j.jsamd.2021.05.004.

(20) Way, A.; Luke, J.; Evans, A. D.; Li, Z.; Kim, J.-S.; Durrant, J. R.; Lee, H. K. H.; Tsoi, W. C. Fluorine Doped Tin Oxide as an Alternative of Indium Tin Oxide for Bottom Electrode of Semi-Transparent Organic Photovoltaic Devices. *AIP Adv.* **2019**, *9* (8), 085220. https://doi.org/10.1063/1.5104333.

(21) Sarma, B.; Barman, D.; Sarma, B. K. AZO (Al:ZnO) Thin Films with High Figure of Merit as Stable Indium Free Transparent Conducting Oxide. *Appl. Surf. Sci.* **2019**, *479* (September 2018), 786–795. https://doi.org/10.1016/j.apsusc.2019.02.146.

(22) Dhage, S. R.; Badgujar, A. C. Transparent Conducting Al:ZnO Thin Films on Large Area by Efficient Cylindrical Rotating DC Magnetron Sputtering. *J. Alloys Compd.* **2018**, *763*, 504–511. https://doi.org/10.1016/j.jallcom.2018.05.234.

(23) Badgujar, A. C.; Yadav, B. S.; Jha, G. K.; Dhage, S. R. Room Temperature Sputtered Aluminum-Doped ZnO Thin Film Transparent Electrode for Application in Solar Cells and for Low-Band-Gap Optoelectronic Devices. *ACS Omega* **2022**, *7* (16), 14203–14210. https://doi.org/10.1021/acsomega.2c00830.

(24) Pung, S.-Y.; Choy, K.-L.; Hou, X.; Shan, C. Preferential Growth of ZnO Thin Films by the Atomic Layer Deposition Technique. *Nanotechnology* **2008**, *19* (43), 435609. https://doi.org/10.1088/0957-4484/19/43/435609.

(25) Garcia, A. J. L.; Jalabert, T.; Pusty, M.; Defoor, V.; Mescot, X.; Montanino, M.; Sico, G.; Loffredo, F.; Villani, F.; Nenna, G.; Ardila, G. Size and Semiconducting Effects on the Piezoelectric Performances of ZnO Nanowires Grown onto Gravure-Printed Seed Layers on Flexible Substrates. *Nanoenergy Adv.* **2022**, *2* (2), 197–209. https://doi.org/10.3390/nanoenergyadv2020008.

(26) Lee, S.; Hinchet, R.; Lee, Y.; Yang, Y.; Lin, Z. H.; Ardila, G.; Montès, L.; Mouis, M.; Wang, Z. L. Ultrathin Nanogenerators as Self-Powered/Active Skin Sensors for Tracking Eye Ball Motion. *Adv. Funct. Mater.* **2014**, *24* (8), 1163–1168. https://doi.org/10.1002/adfm.201301971.

(27) Briscoe, J.; Dunn, S. Piezoelectric Nanogenerators - a Review of Nanostructured Piezoelectric Energy Harvesters. *Nano Energy* **2015**, *14*, 15–29. https://doi.org/10.1016/j.nanoen.2014.11.059.

(28) Tao, R.; Parmar, M.; Ardila, G.; Oliveira, P.; Marques, D.; Montès, L.; Mouis, M. Performance of ZnO Based Piezo-Generators under Controlled Compression. *Semicond. Sci. Technol.* **2017**, *32* (6), 064003.

(29) Consonni, V.; Feuillet, G.; Gergaud, P. Plasticity Induced Texture Development in Thick Polycrystalline CdTe: Experiments and Modeling. *J. Appl. Phys.* **2008**, *103* (6). https://doi.org/10.1063/1.2895382.

(30) Bui, Q. C.; Ardila, G.; Sarigiannidou, E.; Roussel, H.; Jiménez, C.; Chaix-Pluchery, O.; Guerfi, Y.; Bassani, F.; Donatini, F.; Mescot, X.; Salem, B.; Consonni, V. Morphology Transition of ZnO from Thin Film to Nanowires on Silicon and Its Correlated Enhanced Zinc Polarity Uniformity and Piezoelectric Responses. *ACS Appl. Mater. Interfaces* **2020**, *12* (26), 29583–29593. https://doi.org/10.1021/acsami.0c04112.

(31) Luka, G.; Wachnicki, L.; Witkowski, B. S.; Krajewski, T. A.; Jakiela, R.; Guziewicz, E.; Godlewski, M. The Uniformity of Al Distribution in Aluminum-Doped Zinc Oxide Films

Grown by Atomic Layer Deposition. *Mater. Sci. Eng. B* **2011**, *176* (3), 237–241. https://doi.org/10.1016/j.mseb.2010.11.014.

(32) Wu, Y.; Cao, F.; Ji, X. Optical and Electrical Properties of Al-Doped ZnO Thin Films by Atomic Layer Deposition. *J. Mater. Sci. Mater. Electron.* **2020**, *31* (20), 17365–17374. https://doi.org/10.1007/s10854-020-04292-9.

(33) Lin, S.; Huang, J.; Sajgalik, P. The Properties of Heavily Al-Doped ZnO Films before and after Annealing in the Different Atmosphere. *Surf. Coat. Technol.* **2004**, *185* (2–3), 254–263. https://doi.org/10.1016/j.surfcoat.2003.12.007.

(34) Wang, A.; Chen, T.; Lu, S.; Wu, Z.; Li, Y.; Chen, H.; Wang, Y. Effects of Doping and Annealing on Properties of ZnO Films Grown by Atomic Layer Deposition. *Nanoscale Res. Lett.* **2015**, *10*, 75. https://doi.org/10.1186/s11671-015-0801-y.

(35) Birkholz, M. *Thin Film Analysis by X-Ray Scattering*; Wiley-VCH, 2005.

(36) Christman, J. A.; Woolcott, R. R.; Kingon, A. I.; Nemanich, R. J. Piezoelectric Measurements with Atomic Force Microscopy. *Appl. Phys. Lett.* **1998**, *73* (26), 3851–3853. https://doi.org/10.1063/1.122914.

(37) Zhao, M.; Wang, Z.; Mao, S. X. Piezoelectric Characterization of Individual Zinc Oxide Nanobelt Probed by Piezoresponse Force Microscope. *Nano Lett.* **2004**, *4* (4), 587–590.

(38) Ghosh, M.; Rao, M. G. Growth Mechanism of ZnO Nanostructures for Ultra-High Piezoelectric D33 Coefficient. *Mater. Express* **2013**, *3* (4), 319–327. https://doi.org/10.1166/mex.2013.1134.

(39) Wang, Q.; Qiu, Y.; Yang, D.; Li, B.; Zhang, X.; Tang, Y.; Hu, L. Improvement in Piezoelectric Performance of a ZnO Nanogenerator by Modulating Interface Engineering of CuO-ZnO Heterojunction. *Appl. Phys. Lett.* **2018**, *113* (5). https://doi.org/10.1063/1.5035309.

(40) Pradel, K. C.; Wu, W.; Ding, Y.; Wang, Z. L. Solution-Derived ZnO Homojunction Nanowire Films on Wearable Substrates for Energy Conversion and Self-Powered Gesture Recognition. *Nano Lett.* **2014**, *14* (12), 6897–6905. https://doi.org/10.1021/nl5029182.

(41) Li, G.; Zhao, X.; Jia, X.; Li, S.; He, Y. Characterization of Impact Ionization Coefficient of ZnO Based on a P-Si/i-ZnO/n-AZO Avalanche Photodiode. *Micromachines* **2020**, *11* (8). https://doi.org/10.3390/MI11080740.

(42) Lopez Garcia, A. J.; Mouis, M.; Consonni, V.; Ardila, G. Dimensional Roadmap for Maximizing the Piezoelectrical Response of ZnO Nanowire-Based Transducers: Impact of Growth Method. *Nanomaterials* **2021**, *11* (4), 941. https://doi.org/10.3390/nano11040941.

(43) Jalabert, T.; Pusty, M.; Mouis, M.; Ardila, G. Investigation of the Diameter-Dependent Piezoelectric Response of Semiconducting ZnO Nanowires by Piezoresponse Force Microscopy and FEM Simulations. *Nanotechnology* **2023**, *34*, 115402.

(44) Garcia, A. J. L.; Mouis, M.; Jalabert, T.; Cresti, A.; Ardila, G. Length and Polarity Dependent Saturation of the Electromechanical Response of Piezoelectric Semiconducting Nanowires. *J. Phys. D. Appl. Phys.* **2023**, *56* (12), 125301.